Available online at www.sciencedirect.com

SciVerse ScienceDirect

Ceramics International 39 (2013) 5553–5559

CERAMICS INTERNATIONAL

www.elsevier.com/locate/ceramint

Crystallization kinetics and dielectric characterization of CeO_2-added $BaO–SrO–Nb_2O_5–B_2O_3–SiO_2$ glass-ceramics

Tao-yong Liu[a], Guo-hua Chen[a,b,*], Jun Song[a], Chang-lai Yuan[a,b]

[a]School of Materials Science and Engineering, Guilin University of Electronic Technology, Guilin 541004, China
[b]Guangxi Key Laboratory of Information Materials, Guilin University of Electronic Technology, Guilin 541004, China

Received 9 November 2012; received in revised form 16 December 2012; accepted 19 December 2012
Available online 28 December 2012

Abstract

Glass-ceramic materials of the $SrO–BaO–Nb_2O_5–B_2O_3–SiO_2$ system, with various amounts of CeO_2 added, have been prepared by conventional melt casting followed by controlled crystallization. The effect of CeO_2 addition on crystallization kinetics has been explored for dielectric applications. The addition of CeO_2 to the glass-ceramics decreases the activation energy of crystallization and enhances the dielectric constant as well as breakdown strength remarkably. Glass-ceramic with a dielectric constant of 49, breakdown strength of 1250 kV/mm and energy storage density of 3.39 J/cm^3 could be achieved, so this is promising in high energy storage density dielectrics.

Keywords: D. Glass-ceramics; Dielectrics; Rare earth

1. Introduction

Glass-ceramic materials, which are prepared by first obtaining a glass matrix by melt casting [1] and then precipitating a crystal phase in the glass matrix during subsequent heat treatment [2], are replacing conventional ceramics as materials for the application of high energy density dielectrics. Although having high dielectric constant, conventional ceramics have low breakdown strength (~10 kV/mm) due to the presence of residual pores. This kind of defect is formed during solid-state reactions [3] and is difficult to eliminate. In contrast to conventional ceramics, glass-ceramics exhibit the advantages of having both high dielectric constant and high breakdown strength [4]. The energy storage density for dielectric capacitors grows linearly with the dielectric constant and quadratically with the breakdown strength [5], so the glass-ceramic materials possess the potential to achieve a much higher energy storage density.

There have been a large number of investigations of high dielectric constant and high breakdown strength glass-ceramics containing ferroelectric phase such as barium titanate and strontium barium niobate (SBN) [6–8]. Most current glass-ceramics systems for high energy storage are based on silica glass, which often need to be melted above 1500 °C in order to gain superior performance. Shyu et al. and Shyu and Wang [9–10] reported on the densification, crystallization, and dielectric and ferroelectric properties of the $SrO–BaO–Nb_2O_5–SiO_2$ glass-ceramic system and devised a method of sintering compacted glass powders to synthesize glass-ceramics. Rangarajan et al. [11] reported the results of crystallization and the temperature dependence of capacitance in the glass-ceramic system of $Na_2O–BaO–Nb_2O_5–SiO_2$ (BNNS). Recently, Zhou et al. [12] found that the addition of 1 mol% Gd_2O_3 to BNNS glass-ceramic system changed the dielectric constant and breakdown strength remarkably. Sohn et al. [13] and Chen and Liu [14] reported that the addition of CeO_2 effectively reduced the viscosity and promoted the crystallization in the $MgO–Al_2O_3–SiO_2$ system

*Corresponding author at: School of Materials Science and Engineering, Guilin University of Electronic Technology, Guilin 541004, China. Tel.: +86 7732291434; fax: +86 7732290129.
E-mail addresses: cgh1682002@163.com, chengh@guet.edu.cn (G.-h. Chen).

0272-8842/$ - see front matter © 2012 Elsevier Ltd and Techna Group S.r.l. All rights reserved.
http://dx.doi.org/10.1016/j.ceramint.2012.12.069

glasses. As far as we know, studies on SrO–BaO–Nb_2O_5–B_2O_3–SiO_2 glass-ceramics with rare earth oxides are very few.

In this work, CeO_2 is selected as an additive to the SrO–BaO–Nb_2O_5–B_2O_3–SiO_2 glass-ceramic materials with the aim of investigating the influence of CeO_2 addition on crystallization, microstructure, dielectric properties, *P–E* hysteresis loops and energy storage density of the SrO–BaO–Nb_2O_5–B_2O_3–SiO_2 glass-ceramics.

2. Experimental procedure

Powders of analytical reagent grade, comprising $BaCO_3$ (+99.5%), Sr_2CO_3 (+99.5%), Nb_2O_5 (+99.5%), H_3BO_3 (+99.5%), SiO_2 (+99.0%) and CeO_2 (+99.99%), were used as the starting materials. The nominal composition of the starting glass was 21BaO–21SrO–18Nb_2O_5–10B_2O_3–30SiO_2 (mol%). CeO_2 was added to the starting glass in different amounts (mol%), and these compositions were named G0, G1, G2, G3, G4 and G5. The detailed compositions of the glasses are listed in Table 1. The glass-ceramics were prepared by mixing the respective oxide powders and melting them in a corundum crucible in air at 1450 °C for 1 h. The melt was quickly removed from the furnace, poured onto pre-heated copper plate and pressed to form glass sheets with a thickness of about 2 mm. Then, the as-quenched glasses were annealed at 600 °C for 10 h to remove residual stresses and furnace-cooled to room temperature. Glass-ceramics were formed by heat treating these glasses in air at 800 °C for 2 h with a heating rate of 3.5 °C/min based on differential thermal analysis (DTA).

The glass crystallization temperatures were determined by using differential thermal analyses (Model STA-449-F3-Jupiter, Netzsch). Approximately 10 mg of ground glass was used for DTA measurement from 200 °C to 840 °C at a rate of 10 K/min in air. Each sample was examined by various heating rates (5 °C, 10 °C, 15 °C, and 20 °C/min). The activation energy and Avrami exponent (*n*) were calculated according to the data of DTA. Glass-ceramics were examined by an X-ray diffraction diffractometer (XRD) (Model D8-Advance, Bruker) at room temperature in order to investigate the phase evolution. The microstructure of these crystallized samples was analyzed using a scanning electron microscope (SEM) (Model JSM 5610LV, JEOL). For electrical measurements, these samples were polished to achieve parallel, smooth faces, and silver electrodes were sputtered on both faces. The measurements of dielectric constant and dielectric loss for glass-ceramics were performed using a precision multifunction LCR meter (Model HP4292A, Agilent) at room temperature. For dielectric breakdown strength (BDS) measurements, a dc field load was applied to the sample with 0.08–0.10 mm thickness in silicon oil using a high voltage power source (Model MARX, Tianjin Dongwen Company, China). A dc voltage ramp of about 1 kV/s was applied to the specimens until dielectric breakdown. The point where a spike in current was observed was used to identify the dielectric breakdown. At least 10 specimens were used for each composition during BDS testing.

3. Results and discussion

3.1. Crystallization kinetics

DTA was used to analyze the crystallization kinetics of glasses. Peak crystallization temperatures of glasses heated at different heating rates ranging from 5 °C to 20 °C are

Table 1
Composition of the glass-ceramics with CeO_2 added (mol%).

Symbol	BaO	SrO	Nb_2O_5	B_2O_3	SiO_2	CeO_2
G0	21	21	18	10	30	0
G1	21	21	18	10	30	0.90
G2	21	21	18	10	30	2.65
G3	21	21	18	10	30	4.40
G4	21	21	18	10	30	6.20
G5	21	21	18	10	30	8.80

Table 2
Peak crystallization temperatures (T_p) of the glasses at different heating rates.

Symbol	T_p (K)			
	α=5 K/min	α=10 K/min	α=15 K/min	α=20 K/min
G0	1081.25	1099.15	1110.15	1118.55
G1	1074.15	1091.15	1104.25	1112.25
G2	1073.15	1090.15	1104.15	1112.15
G3	1069.15	1087.15	1101.15	1110.15
G4	1067.15	1085.15	1100.15	1108.15
G5	1069.15	1086.15	1101.15	1109.15

shown in Table 2. By increasing the content of CeO_2, the exothermic peak temperatures of glasses first decrease and then increase obviously. It means that the additions of CeO_2 make this system easier to crystallize [15]. Increasing the heating rate results in an increase in the peak crystallization temperature (T_p), and from this shift, the activation energy of crystallization could be determined from the Kissinger equation [16], as follows:

$$\ln\left(\frac{T_p^2}{\Phi}\right) = \frac{E}{RT_p} + \text{constant} \quad (1)$$

where T_p is the temperature at which the maximum of the DTA crystallization peak exotherm is noted, Φ is the heating rate, R is the gas constant, and E is the activation energy for crystallization. According to the equation, a plot of ln (T_p^2/Φ) versus $1/T_p$ yields a straight line in which the slopes are proportional to the activation energy of crystallization. These plots are shown in Fig. 1 and the values of crystallization activation energy are shown in Table 3. It is found that the activation energy first decreases and then increases with the increase in the contents of CeO_2. In general, cerium acts as a network modifier in the glass because it may have six or eight coordination numbers and its ionic field strength is 0.83 [17]. Hence, the glass structure becomes looser with increase in the amount of cerium ions, which can largely increase the number of non-bridging oxygen by forming [CeO_6] or [CeO_8] unit. The relative low activation energies of the samples with CeO_2, therefore, are attributed to the addition of CeO_2, the network modifier. On the other hand, the relative high activation energy of G0 is due to the high contents of SiO_2 and B_2O_3 in the glass

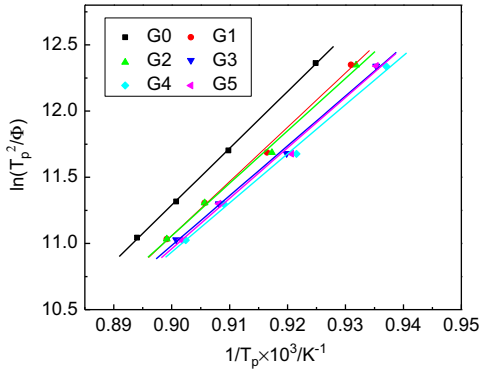

Fig. 1. Plots of ln (T_p^2/Φ) versus $1/T_p$.

Table 3
Crystallization kinetic parameters of the glasses as determined by DTA.

Symbol	E (kJ/mol)	Avrami parameter (n)
G0	357	0.71
G1	341	0.82
G2	329	0.81
G3	313	0.93
G4	306	0.99
G5	317	0.68

matrix. It means that the addition of appropriate amount of CeO_2 indeed decreases the activation energy of crystallization and enhances the crystallization of the crystal phase from the glass matrix.

Additionally, the value of the Avrami exponent, n, can be determined from the DTA results by Ozawa's equation [18], as follows:

$$\left\{\frac{d\ln[-\ln(1-x)]}{d\ln \Phi}\right\} = -n \quad (2)$$

where n is the Avrami parameter, and x is the volume fraction crystallized which is given as $x=(A/A_0)$, where A_0 is the total area of the exotherm between the temperature T_i at which crystallization just begins and T_f at which the crystallization is completed. A is the area between T_i and T. Φ is the heating rate. The slope of the plot of ln $(-\ln(1-x))$ versus ln(Φ) can be obtained from the above equation. The average values of n are shown in Table 3. The values of n for all samples are close to 1, which indicates that the crystallization mechanism of the glass-ceramics is surface crystallization. It is noted that the activation energy of all samples is close to the diffusion energy of Sr^{2+} (255 kJ/mol) and B^{3+} (280–350 kJ/mol) [19]. Consequently, it is inferred that the diffusion controlled growth may play a main role in these glasses.

3.2. Microstructure

Fig. 2 shows the XRD patterns of the glass-ceramics heat treated at 800 °C for 2 h. By heat treatment, intense diffraction peaks, which could be ascribed to ($Sr_{0.75}Ba_{0.25}$) Nb_2O_6 crystal, are observed. However, a trace of secondary phase $Ba_3Nb_6Si_4O_{26}$ also occurs for all samples. In these samples with CeO_2, the diffraction peaks become obvious and intense, which indicates the gradual formation of ($Sr_{0.75}Ba_{0.25}$) Nb_2O_6 crystal. Fig. 3 shows the microstructure of the glass-ceramics heat treated at 800 °C for 2 h. In Fig. 3, the microstructure of the glass-ceramics with different CeO_2 content is quite different. In the microstructures of G0, pores and no-uniform microstructure can be seen clearly. From G0 to G4, the increase in the content of CeO_2 improves the crystallization obviously. This result

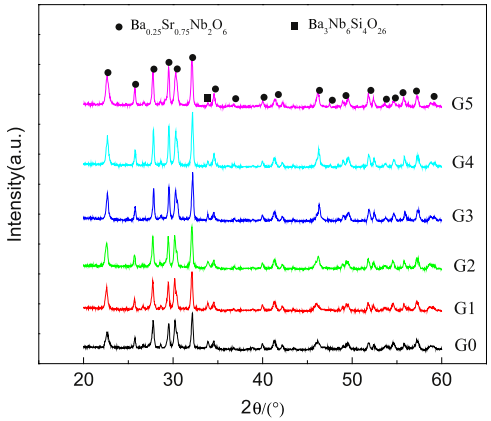

Fig. 2. XRD patterns of the glasses heat treated at 800 °C for 2 h.

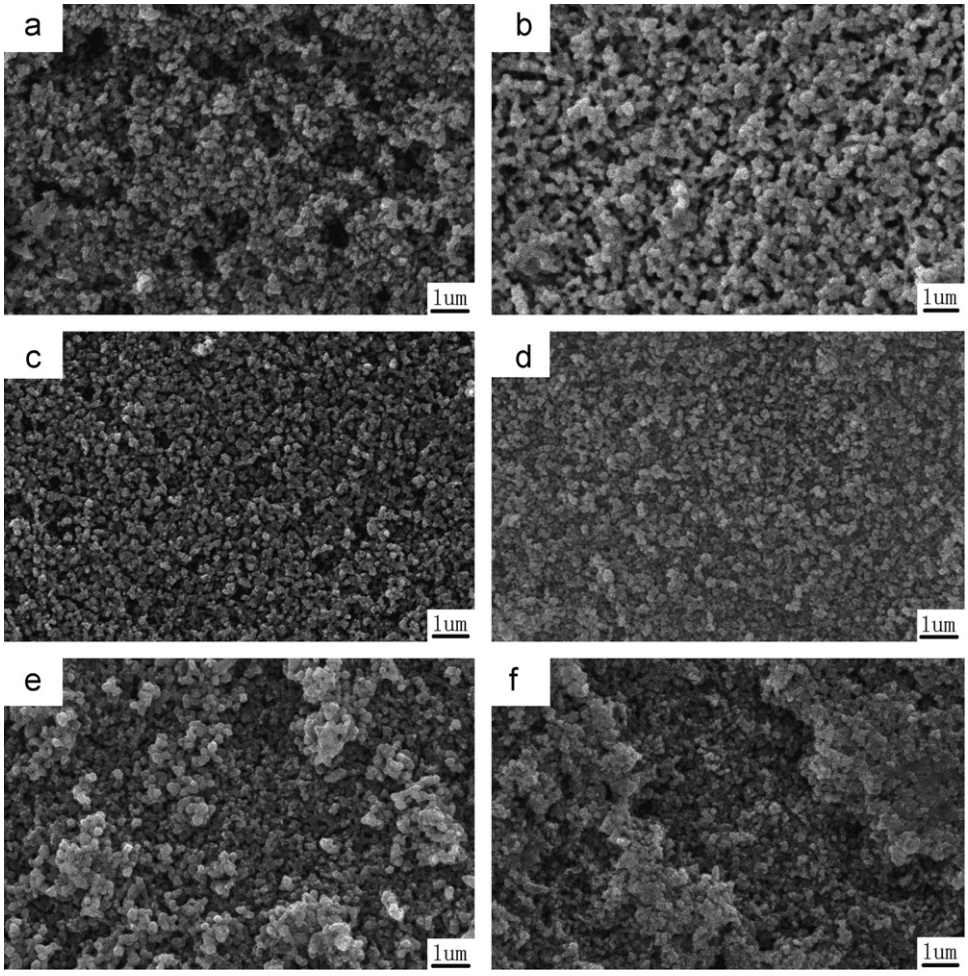

Fig. 3. Scanning electron micrographs of (a) G0, (b) G1, (c) G2, (d) G3, (e) G4, and (f) G5 glass-ceramics heat treated at 800 °C for 2 h.

is consistent with DTA data where the values of the activation energy decrease from G0 to G4 gradually. Especially in G3 sample shown in Fig. 3d, the uniform and dense microstructure can be observed. However, further increase in the content of CeO_2 deteriorates the uniform microstructure shown in Fig. 3e and f. The average grain sizes of all glass-ceramics are in the range of 100–250 nm, and the average grain sizes slightly increase for G4 and G5 samples with higher amounts of CeO_2.

3.3. Dielectric properties

Fig. 4 illustrates the relative dielectric constant and dielectric loss measured at 1 kHz as a function of the content of CeO_2. When the content of CeO_2 is <6.2 mol%, the dielectric constant increases with the increase in the addition of CeO_2. However, further increase in the content of CeO_2 leads to some decrease in the value of dielectric constant. It is consistent with the variation of the XRD in Fig. 3 from G0 to G5. The dielectric loss decreases slightly at low content of CeO_2. When the content of CeO_2 is >4.4 mol%, the dielectric loss increases obviously. In a word, all glass-ceramic materials have a low level of the dielectric loss.

The distribution of the electrical breakdown strength (BDS) can be plotted by the two-parameter Weibull function [20], which is given by

$$X_i = \ln(E_i) \tag{3}$$

$$Y_i = \ln\left(-\ln\left(\frac{1-i}{(n+1)}\right)\right) \tag{4}$$

where E_i is the specific breakdown field of each specimen, n is the sum of specimens of each composition, and i is the serial number of each specimen, which are arranged in ascending order of BDS values so that

$$E_1 \le E_2 \le E_3 \le E_i \le E_n \tag{5}$$

The two-parameter Weibull distribution function Y_i (X_i) should be a line in the coordinate system. The slope of the line is the shape parameter β, which is related to the range of the BDS. The intercept on the X-axis is $\ln \alpha$, where α is the scale parameter which can reflect the magnitude of BDS. When $\beta > 1.0$, it means that the failure could be

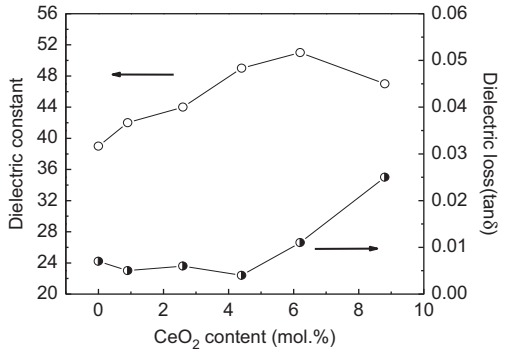

Fig. 4. Dielectric constant (ε_r) and dielectric loss ($\tan\delta$) of the glass-ceramics as a function of the addition of CeO_2.

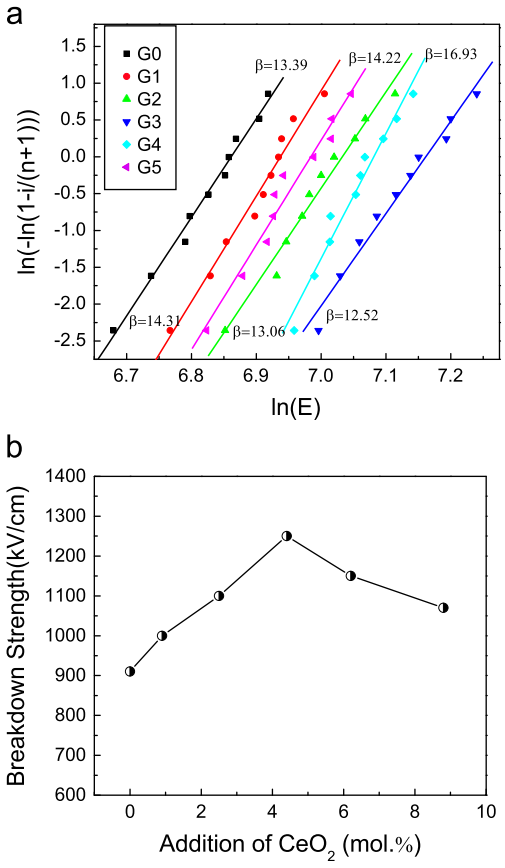

Fig. 5. Weibull plots of dielectric breakdown strength (a) and average breakdown strength (b) of the glass-ceramics with different amounts of CeO_2 heat treated at 800 °C for 2 h.

analyzed by the Weibull model. The greater the β, the more reliable the model would be. In Fig. 5(a), the β values of the glass-ceramics are >1 and the breakdown data of glass-ceramics follow the Weibull distribution. The magnitude of BDS could be reflected by the scale parameter. The average breakdown strength (α) of glass- ceramics is shown in Fig. 5(b).

From Fig. 5(b), it is observed that the breakdown strength of G0 sample without CeO_2 is 910 kV/cm and the breakdown strength of other samples containing CeO_2 is improved remarkably. All samples containing CeO_2 have high breakdown strength of ≥ 1000 kV/cm. It is observed that G3 sample has the highest breakdown strength of 1250 kV/cm, possibly due to the homogeneous and dense microstructure together with fine grain as shown in Fig. 3d. However, too much CeO_2 is not helpful to enhance the breakdown strength. Generally, the breakdown strength of dielectric materials depends on several factors, including porosity, grain size, and extrinsic measurement conditions such as sample thickness, sample area, and electrode configuration [21–23]. Based on the above analysis, it is suggested that the improvement of breakdown strength is primarily due to the uniform microstructure and the decrease of porosity.

The polarization–electric field (P–E) hysteresis loops of the glass-ceramics are plotted in Fig. 6. From Fig. 6, it can be seen that the polarization shows a gradual increase firstly and then slightly decreases with the increase in the addition of CeO_2, which is in agreement with the dielectric constant shown in Fig. 4. Additionally, the remnant polarization of G0 sample is 0.019 $\mu C/cm^2$, while the remnant polarization values of G1, G2, G3, G4, and G5 samples are 0.037, 0.041, 0.047, 0.065, and 0.042 $\mu C/cm^2$, respectively. This result may be explained by the formation of ferroelectric phases increased from the glass matrix. Although small remnant polarization is existent, the P–E characteristics do not show other typical ferroelectric behavior. It means that the glass matrixes still occupy a lot of component in the glass-ceramics. Therefore, the theoretical energy storage density of the glass-ceramics can be calculated as a linear dielectric material.

According to the theory of dielectric physics [24], the energy storage density of linear dielectric materials can be expressed as

$$W = 1/2\varepsilon_0\varepsilon_r E_b^2 \quad (6)$$

where ε_0 and ε_r are the dielectric constant of the vacuum permittivity and relative permittivity, and E_b is the applied electric field where the breakdown occurs. The theoretical energy storage densities of G0, G1, G2, G3, G4, and G5 samples are 1.43, 1.86, 2.35, 3.39, 2.83 and 2.43 J/cm^3, respectively. G3 glass-ceramic sample has the highest energy storage density of 3.39 J/cm^3, which has been attributed to a summation of factors including highly polarizable ions enhancing the real part of complex permittivity, the low loss and the substantially defect-free quality of the glass-ceramics.

4. Conclusion

The crystallization kinetics and dielectric properties of the SrO–BaO–Nb_2O_5–B_2O_3–SiO_2–CeO_2 system have been investigated. The addition of CeO_2 has been found to decrease the activation energy of crystallization and improve the crystallization. Especially, G3 glass-ceramic sample shows the dense and uniform microstructure and the highest breakdown

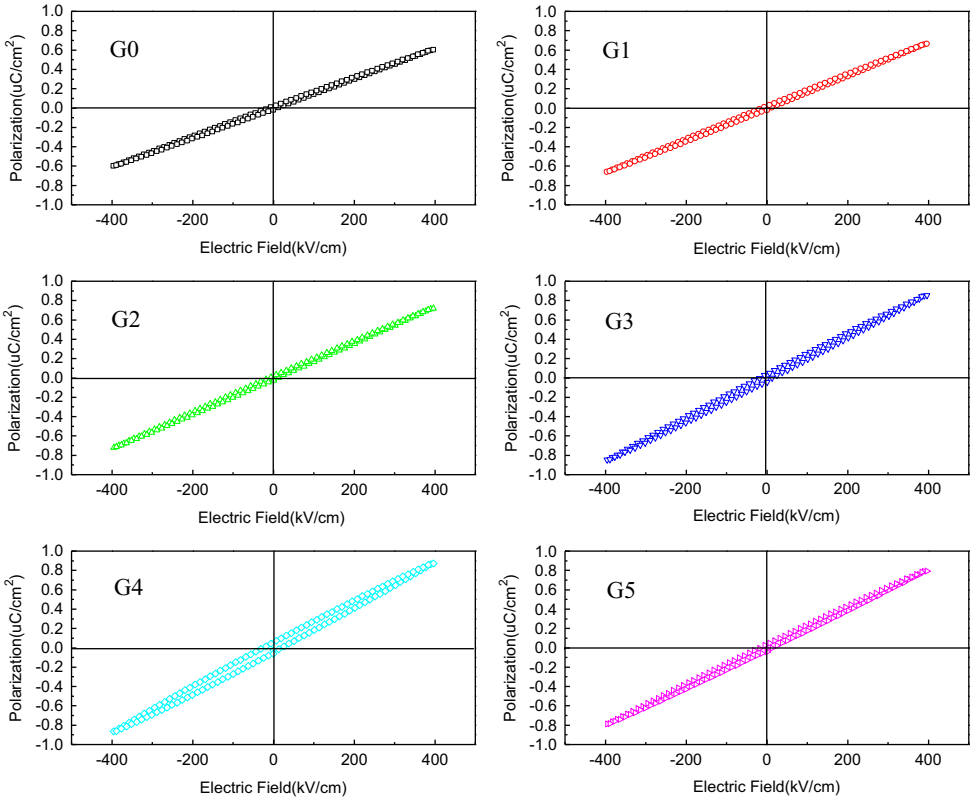

Fig. 6. *P–E* hysteresis loops of the glass ceramics.

strength. The appropriate addition of CeO_2 indeed improves dielectric properties and subsequently increases energy storage density of glass-ceramics. These findings indicate that this glass-ceramics system could be a strong candidate for use in high energy density storage dielectrics.

Acknowledgments

This work was supported by Natural Science Foundation of China (NSFC no. 51162002) and Science and Technology Project of Guangxi Returned Personnel (Contract no. [2012]250)

References

[1] P.W. McMillan, Glass Ceramics, Academic Press, London, 1964.
[2] E.P. Gorzkowski, M.J. Pan, B. Bender, C.C.M. Wu, Glass-ceramics of barium strontium titanate for high energy density capacitors, Journal of Electroceramics 18 (3–4) (2007))269–276.
[3] Q.M. Zhang, L. Wang, J. Luo, Q. Tang, J. Du, Improved energy storage density in barium strontium titanate by addition of BaO–SiO_2–B_2O_3 glass, Journal of the American Ceramic Society 92 (8) (2009) 1871–1873.
[4] A. Herczog, Application of glass-ceramics for electronic components and circuits, IEEE Transactions on Parts Hybrids and Packaging PHP-9 (4) (1973) 247–256.
[5] G.R. Love, Energy storage in ceramic dielectrics, Journal of the American Ceramic Society 73 (2) (1990) 323–328.
[6] Y. Zhang, J.J. Huang, T. Ma, X.R. Wang, C.S. Deng, X.M. Dai, Sintering temperature dependence of energy-storage properties in (Ba, Sr)TiO_3 glass-ceramics, Journal of the American Ceramic Society 94 (6) (2011) 1805–1810.
[7] Z.H. Wu, H.X. Liu, M.H. Cao, Z.Y. Shen, Z.H. Yao, H. Hao, D.B. Luo, Effect of BaO–Al_2O_3–B_2O_3–SiO_2 glass additive on densification and dielectric properties of $Ba_{0.3}Sr_{0.7}TiO_3$ ceramics, Journal of the Ceramic Society of Japan 116 (2) (2008) 345–349.
[8] G.H. Chen, W.J. Zhang, X.Y. Liu, C.R. Zhou, Preparation and properties of strontium barium niobate based glass-ceramics for energy storage capacitors, Journal of Electroceramics 27 (2) (2011) 78–82.
[9] J.J. Shyu, C.H. Chen, Sinterable ferroelectric glass-ceramics containing (Sr, Ba)Nb_2O_6 crystals, Ceramics International 29 (4) (2003) 447–453.
[10] J.J. Shyu, J.R. Wang, Crystallization and dielectric properties of SrO–BaO–Nb_2O_5–SiO_2 tungsten-brone glass-ceramics, Journal of the American Ceramic Society 83 (12) (2003) 3135–3140.
[11] B. Rangarajan, B. Jones, T. Shrout, M. Lanagan, Barium/lead-rich high permittivity glass-ceramics for capacitor applications, Journal of the American Ceramic Society 90 (3) (2007) 784–788.
[12] Y. Zhou, Q.M. Zhang, J. Luo, Q. Tang, J. Du, Structural and dielectric characterization of Gd_2O_3-added BaO–Na_2O–Nb_2O_5–SiO_2 glass-ceramic composites, Scripta Materialia 65 (4) (2011) 296–299.
[13] S.B. Sohn, S.Y. Choi, Y.K. Lee, Controlled crystallization and characterization of cordierite glass-ceramics for magnetic memory disk substrate, Journal of Materials Science 35 (2000) 4815–4821.
[14] G.H. Chen, X.Y. Liu, Fabrication, characterization and sintering of glass-ceramics for low-temperature co-fired ceramic substrates, Journal of Materials Science: Materials in Electronics 15 (9) (2004) 595–600.
[15] B.H. Kim, K.H. Lee, Crystallization and sinterability of cordierite-based glass powders containing CeO_2, Journal of Materials Science 29 (24) (1994) 6592–6598.
[16] H.E. Kissinger, Variation of peak temperatures with heating rate in differential thermal analysis, Journal of Research of the National Bureau of Standards 57 (4) (1956) 217–221.
[17] M.B. Volf, Chemical Approach to Glass, Elsevier Science Publishers, 1984 63–64.

[18] T. Ozawa, Kinetic analysis of derivative curves in thermal analysis, Journal of Thermal Analysis and Calorimetry 2 (3) (1970) 301–324.
[19] C.T. Cheng, M. Lanagan, J.T. Lin, B. Jones, M.J. Pan, Crystallization kinetics and dielectric properties of nanocrystalline lead strontium barium niobates, Journal of Materials Research 20 (2) (2005) 438–446.
[20] A.L. Young, G.E. Hilmas, S.C. Zhang, R.W. Schwartz, Mechanical vs. electrical failure mechanisms in high voltage, high energy density multilayer ceramic capacitors, Journal of Materials Science Letters 42 (14) (2007) 5613–5619.
[21] T. Tunkasiri, G. Rujijanagul, Dielectric strength of fine grained barium titanate ceramics, Journal of Materials Science Letters 15 (20) (1996) 1767–1769.
[22] E.K. Beauchamp, Effect of microstructure on pulse strength of MgO, Journal of the Chinese Ceramic Society 54 (10) (1971) 484–487.
[23] G. Mazzanti, G.C. Montanari, F. Peruzzotti, A. Zaopo, Some remarks regarding the test cells used for electric strength measurement, Electrical Insulation 2 (1996) 474–477.
[24] N.H. Fletcher, A.D. Hilton, B.W. Ricketts, Optimization of energy storage density in ceramic capacitors, Applied Physics 29 (1) (1996) 253–258.